

Development of an arc-shaped precipitation system during the pre-monsoon period in Bangladesh

M. Rafiuddin · Hiroshi Uyeda · Masaya Kato

Received: 3 March 2012 / Accepted: 7 March 2013 / Published online: 22 March 2013
© Springer-Verlag Wien 2013

Abstract A numerical simulation is performed to understand the features and development processes of the arc-shaped precipitation system that dominates in Bangladesh during the pre-monsoon (March–May) period. An arc-shaped precipitation system of 26 April 2002 is simulated using the Cloud Resolving Storm Simulator (CReSS) with a horizontal grid increment of 2 km. The Pennsylvania State University/National Center for Atmospheric Research Mesoscale Model is used for downscaling. Hourly outputs of the finest domain (grid increment of 5 km) of MM5 and National Oceanic and Atmospheric Administration Reynolds weekly mean sea surface temperature data are used as the initial and boundary conditions for CReSS. Younger and more intense cells are formed in the southwestern end of the system. These cells move northeastward and merge with the system producing intense rainfalls. Simulation results indicate that low-level southwesterly or southerly wind brings warm moist air from the Bay of Bengal and helps develop new cells. The propagation speed of the system is 8 m/s, and the northeastern end moves faster than the southwestern end, creating clockwise rotation of the system. The propagation speed and the rotation of the simulated system coincide well with radar observations.

The clockwise rotation of the system can be explained by the stronger (weaker) outflow and weaker (stronger) inflow in the northeastern (southwestern) end. The propagation of the system is attributable to the weak (≤ 7 m/s, storm relative) rear-to-front flow in the moist environment. Thus, the arc-shaped precipitation system common to the pre-monsoon period in Bangladesh develops through a balance of strong southwesterly or southerly moist inflow in the low altitudes below 2 km and relatively weak outflow in the rear of the system.

1 Introduction

In Bangladesh (88.05–92.74°E, 20.67–26.63°N), a notable weather phenomenon is the outburst of severe local convective storms that develop in the north-west part and propagate southeastward, commonly known as “nor’westers” and locally called “Kal-baishakhi” in the Bengal area, during the pre-monsoon period (March–May). These severe local storms often include thunder, lightning, intense rain, hail, and wind gusts, and tornados, and every year such storms lead to extensive agricultural and property damage and the loss of human life. Pre-monsoon precipitation systems play an important role in the socioeconomic development of the agricultural-dependent country of Bangladesh. Thus, it is important to understand the processes by which pre-monsoon precipitation systems develop over the Bangladesh area.

Previous research on pre-monsoon precipitation systems in and around Bangladesh has been conducted mainly in the framework of climatology. Peterson and Mehta (1981) examined tornado activity in Bangladesh and northeastern India and found the highest monthly occurrence frequency in April. Chowdhury and De (1995) reported that the

Responsible editor: M. Kaplan.

M. Rafiuddin (✉)
Department of Physics, Bangladesh University of Engineering
and Technology, Dhaka 1000, Bangladesh
e-mail: rafiuddin@phy.buet.ac.bd; rafii015@yahoo.com

H. Uyeda · M. Kato
Hydrospheric Atmospheric Research Center, Nagoya University,
Nagoya, Japan

frequency of thunderstorms and amount of precipitation are the greatest in the month of May in Bangladesh during the pre-monsoon period. Yamane and Hayashi (2006) used reanalysis data to show that combinations of high Convective Available Potential Energy (CAPE) and moderate shear are favorable for the occurrence of severe local storms during the pre-monsoon period in Bangladesh and northeastern India. Islam and Uyeda (2008) analyzed Tropical Rainfall Measuring Mission (TRMM) data and found that pre-monsoon rainfall is characterized by convective rain with strong intensity that reaches high altitudes and high echo tops. Rafiuddin et al. (2010) used 6 years of radar data to reveal that fast-moving arc-type precipitation systems (having an arc-shaped strong leading edge and a stratiform region behind) dominate in the pre-monsoon period, whereas slow-moving scattered-type systems (groups of poorly organized small individual echoes with less than 50 km as the maximum distance between echoes) dominate in the monsoon period. They showed 160 (80) arc-type (scattered-type) precipitation systems developed from April to May and 70 (362) arc-type (scattered-type) precipitation systems developed from June to September. However, due to the scarcity of data, the development processes, dynamics, and thermodynamics of pre-monsoon precipitation systems in Bangladesh have not been well documented.

A few simulation studies have looked at the features and development processes of pre-monsoon precipitation system in and around Bangladesh. To examine stability indices, Litta and Mohonty (2008) used a mesoscale model to simulate thunderstorm development over eastern India. Their results showed that higher instability indicates the occurrence of a thunderstorm. Kataoka and Satomura (2005) conducted a numerical simulation of precipitation over the Bangladesh region during the monsoon period and explained the development and southward or southwestward propagation of significant squall-line precipitation systems near the southern foot of the Meghalaya Plateau. However, simulation results of Kataoka and Satomura (2005) for system development were not verified with ground-based observations. Although the arc-shaped precipitation system is dominated during the pre-monsoon period, as revealed by Rafiuddin et al. (2010), their development process and features of typical systems have not been clarified because of lack of observational and numerical modeling study. To clarify the features and development processes of a typical pre-monsoon arc-shaped precipitation system, this study with a cloud resolving model examines a case for which almost continuous radar scan data are available.

2 Description of radar and model

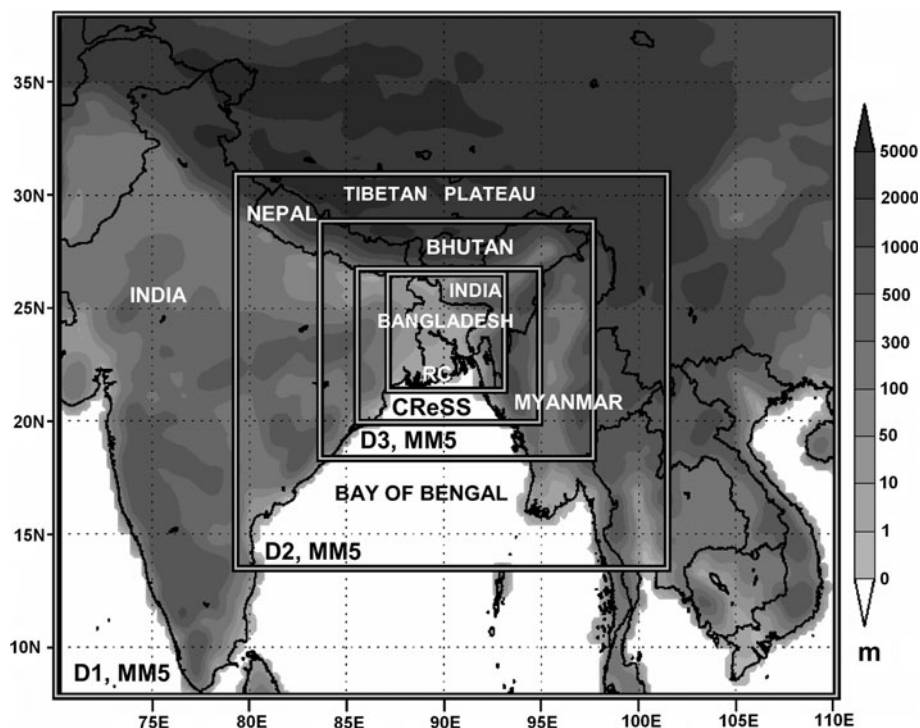
2.1 Radar

An S-band weather radar (wavelength ~ 10 cm, beam width 1.7° , elevation angle 0°) is placed on a building roof at the height of ~ 60 m in the vicinity of Bangladesh Meteorological Department (BMD) office in Dhaka ($23^\circ 42' 0''$ N and $90^\circ 22' 30''$ E) that covers $600 \text{ km} \times 600 \text{ km}$ area (Fig. 1). The regular scanning scheme of the radar is 1 h at 'ON' and 2 h 'PAUSE'. The pixel resolution is $2.5 \text{ km} \times 2.5 \text{ km}$. BMD does not operate radar from 00 LST to 05 LST (LST = UTC + 6 h). BMD radar covers almost the whole of Bangladesh including some neighboring parts of India and Myanmar. Sometimes radar is operated for a few continuous hours without any break. BMD radar collects reflectivity data and automatically converts to the precipitation rate (mm/h) and provides the output only in plan position indicator (PPI) scan in six statuses: 1 ($1 \text{ mm/h} \leq \text{rain rate} < 4 \text{ mm/h}$), 2 ($4 \text{ mm/h} \leq \text{rain rate} < 16 \text{ mm/h}$), 3 ($16 \text{ mm/h} \leq \text{rain rate} < 32 \text{ mm/h}$), 4 ($32 \text{ mm/h} \leq \text{rain rate} < 64 \text{ mm/h}$), 5 ($64 \text{ mm/h} \leq \text{rain rate} < 128 \text{ mm/h}$) and 6 ($128 \text{ mm/h} \leq \text{rain rate}$). There are about 20 PPI scans (2–3 min interval) available during each operation hour.

2.2 Model

This study attempts to simulate an arc-shaped precipitation system that developed on 26 April 2002, using the Cloud Resolving Storm Simulator (CReSS). CReSS model is developed by the Hydrospheric Atmospheric Research Center (HyARC) of Nagoya University, Japan (Tsuboki and Sakakibara 2002). CReSS is a three-dimensional nonhydrostatic and compressible model and includes a bulk cold-rain parameterization and a 1.5-order closure scheme with a turbulent kinetic energy prediction. The prognostic variables are the three components of wind velocity; perturbation of potential temperature and pressure; subgrid-scale turbulent kinetic energy; mixing ratios of vapor (q_v), cloud water (q_c), rain (q_r), cloud ice (q_i), snow (q_s), and graupel (q_g); and the number concentrations of cloud ice (N_i), snow (N_s), and graupel (N_g). In the microphysics of CReSS, six species (water vapor, cloud, ice, rain, snow, and graupel) are considered. Their mixing ratios and the number concentrations of ice, snow, and graupel are predicted. The surface fluxes of the momentum, energy, and surface radiation processes are included with a one-dimensional heat diffusion model in the underground layer for ground temperature prediction.

Fig. 1 Model domains. *D1*, *D2*, *D3*, *CReSS*, and *RC* indicate the areas of MM5 domains 1, 2, and 3 and CReSS and radar coverage, respectively. The horizontal grid increments of *D1*, *D2*, *D3*, and *CReSS* are 45, 15, 5, and 2 km, respectively. Gray shading indicates the topography



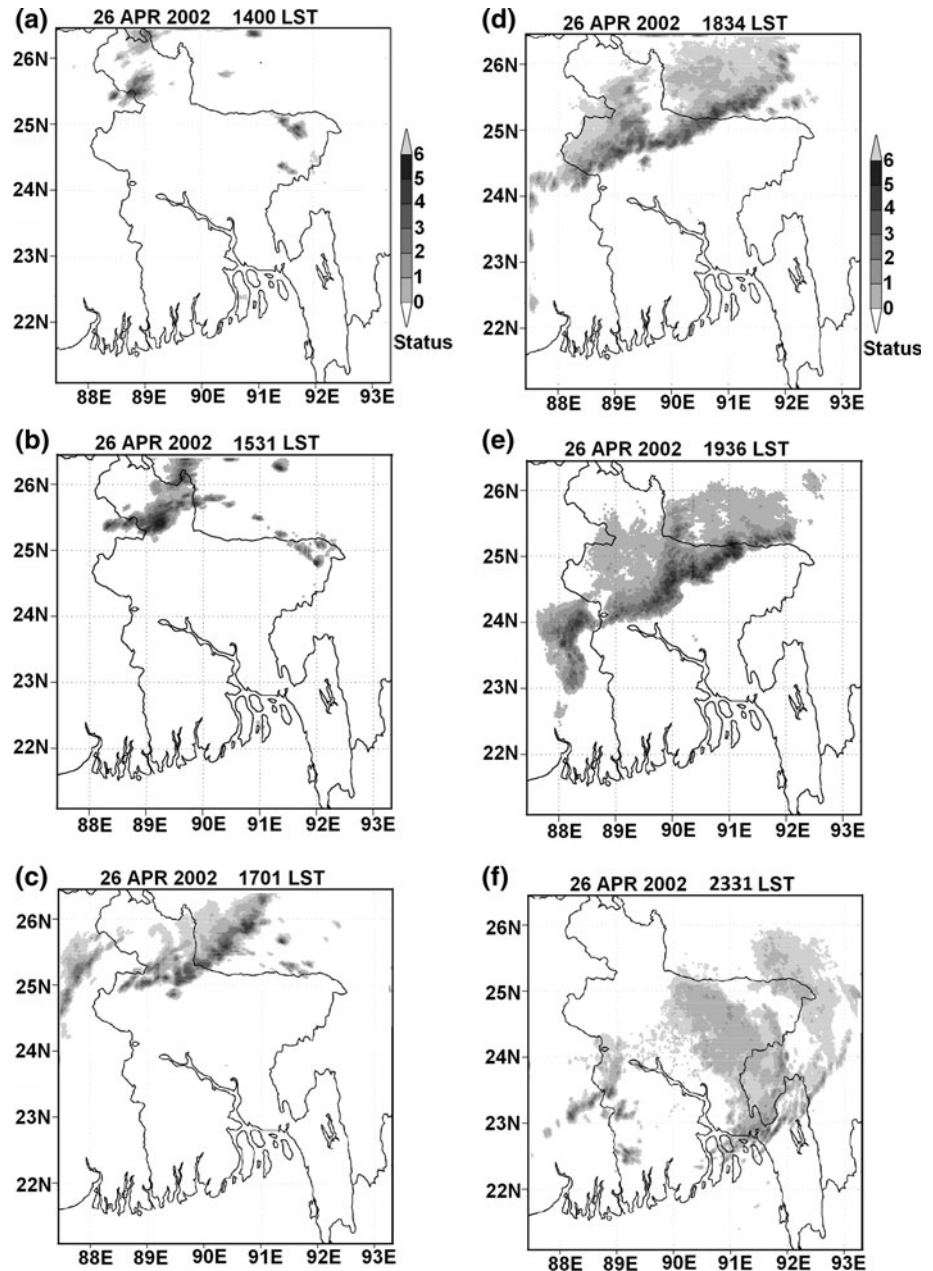
A nonhydrostatic mesoscale model, the Pennsylvania State University/National Center for Atmospheric Research Mesoscale Model (PSU/NCAR MM5; Dudhia 1993), is used for downscaling. Japanese 25-year Reanalysis (JRA-25) data of 1.25-degree resolution and National Oceanic and Atmospheric Administration (NOAA) Reynolds weekly mean sea surface temperature (SST) data are used for the initial and boundary conditions of MM5. MM5 simulation has been performed for three domains (*D1*, *D2*, and *D3* in Fig. 1) with horizontal grid increments of 45, 15, and 5 km, respectively. The top of MM5 is 10 hPa, with 23 sigma levels for all three domains. Lambert conformal projection is used in Grell's (1993) scheme for convective parameterization with a shallow cloud option. The explicit moisture scheme is simple ice (Dudhia 1989) and Medium Range Forecast (MRF) scheme (Hong and Pan 1996) is used for the planetary boundary layer (PBL). The MM5 simulation starts at 0000 LST (LST = UTC + 6) on 26 April 2002 and continues for 42 h. Hourly outputs of *D3* and NOAA Reynolds weekly mean SST are used to specify the initial and boundary conditions for CReSS. CReSS is run for a single domain (Fig. 1) with a horizontal grid increment of 2 km and 70 vertical layers with the average stretched grid increments of 400 m (200 m at the lowest level). Lambert conformal projection is used in a bulk cold-rain precipitation scheme. CReSS simulation starts at 0600 LST on 26 April 2002 and continues for 36 h.

3 Overview of the arc-shaped precipitation system

Radar observed the development of an arc-shaped precipitation system over northwestern Bangladesh on 26 April 2002 (Fig. 2a–f). Radar PPI scans show that two systems appeared over the northwestern side of Bangladesh at around 1400 LST on 26 April (Fig. 2a). By 1531 LST (Fig. 2b), these systems intensified and organized into a line that moved southeastward and developed into an intensified arc-shaped precipitation system at 1701 LST (Fig. 2c). The system elongated from the southwest to northeast and propagated southeastward. Another system developed at 1701 LST (Fig. 2c) in the west side of the first system. These two systems merged and intensified at 1834 LST (Fig. 2d). The system became mature at 1936 LST, with a length of ~530 km (Fig. 2e). The arc-shaped precipitation system propagated southeastward and dissipation started at 2147 LST. The system became very weak by 2331 LST (Fig. 2f).

Figure 3 shows time series of new cells development of the system. These cells develop in the southwestern end of the system and move northeastward. On the basis of the radar observations, this arc-shaped precipitation system reached its initial, mature, and decaying stages at 1531, 1930, and 2147 LST, respectively (Fig. 4a–c). The system had a lifetime of nearly 10 h.

Fig. 2 The development of systems on 26 April 2002 observed by radar PPI at **a** 1400 LST, **b** 1531 LST, **c** 1701 LST, **d** 1834 LST, **e** 1936 LST and **f** 2331 LST



4 Simulation results

4.1 Overview of the simulated system development

Horizontal distributions of the mixing ratio of precipitation ($q_r + q_s + q_g$) and wind field of the pre-monsoon arc-shaped precipitation system simulated by CReSS are shown in Fig. 4d–f. In the simulation, the system appears outside of the radar domain, with location shift and time delay. The system appears within the radar domain at 1700 LST on 26 April 2002. The simulated system attains an arc-shaped precipitation around 1800 LST and a length of approximately 150 km. The arc shape of the system

increases, and it propagates southeastward around 2100 LST. Within this time, the system becomes more intense, grows to approximately 400 km in length, and extends into the stratiform region. Around 2300 LST, the system further extends in the stratiform region and has a length of approximately 550 km. At this time, the convective region of the system becomes weak. The developing, mature, and decaying stages of the system are identified as occurring at 1800, 2100, and 2300 LST, respectively (note in this study, for simulation, we show developing stage because the simulated initial stage occurred outside the radar domain) (Fig. 4d–f); these times correspond to the times of the radar PPI scans shown in Fig. 4a–c. From Fig. 4, it is clear that

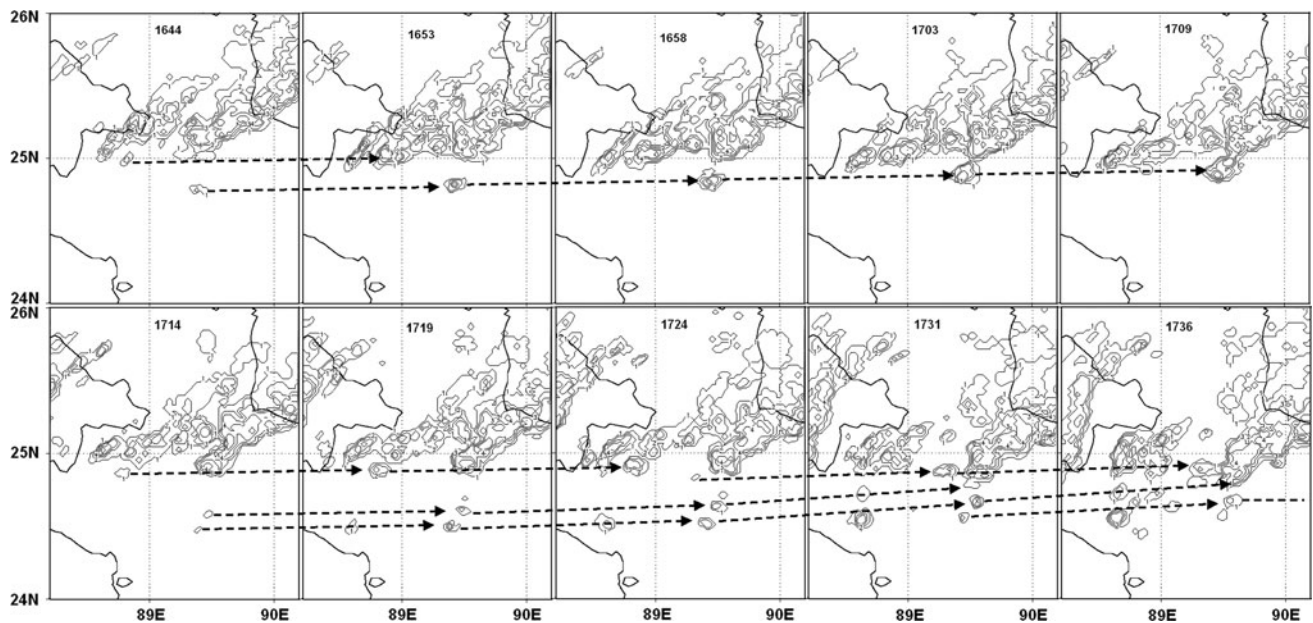


Fig. 3 Time series of cells development observed by radar

the model simulation captures the overall horizontal structure of the system. The system is oriented southwest to northeast.

4.2 Characteristics of the simulated system

Figure 5 shows the hourly time series of the leading edge of the system. The propagation path, speed and direction through the lifetime of the system are close to those observed by radar (Fig. 5a). The average simulated propagation speed is approximately 8 m/s, whereas the radar-observed speed is about 7 m/s. Figure 5 shows that the northeastern end of the system moves faster than does the southwestern end, and the system rotates clockwise as the system progresses from the initial to decaying stages. Table 1 presents characteristics such as the length, propagation speed, and direction at different stages. The simulated characteristics (length, propagation speed, and direction) well match those observed by radar.

4.3 Dynamical and thermodynamical structure of the simulated system

4.3.1 Horizontal structure

Figure 6a–c shows the model-simulated temperature and wind field distribution during the developing, mature, and decaying stages of the system at 1 km height. The temperature at the southwestern side is higher than that at the northeastern side. Behind the leading edge of the system, shown by mixing ratio of precipitation (contours above

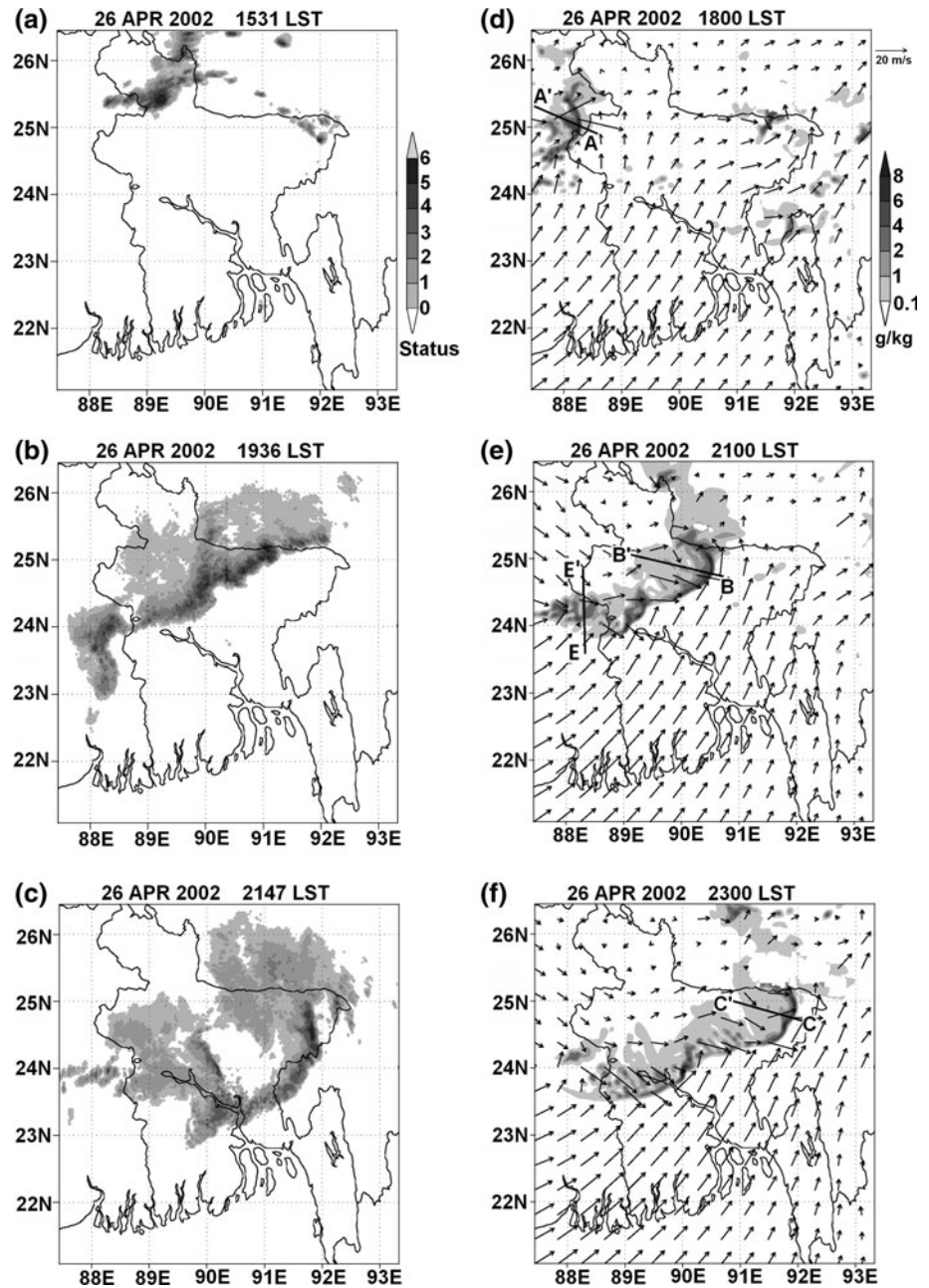
4 g/kg), the low temperature (≤ 291 K) area at 1 km height is more extended at 2300 LST (Fig. 6c) than at 1800 LST (Fig. 6a) on 26 April 2002. Temperature drops of approximately 4 and 3 K are found in the northeastern and southwestern ends of the system, respectively. Behind the system, the area of the low temperature region is larger at the northeastern end than at the southwestern end as the system progresses from its initial to decaying stages.

Figure 6d–f shows the relative humidity distribution during the developing, mature, and decaying stages of the system at 1 km height. The low-level (1 km) relative humidity ahead of the leading edge of the system is very high ($>95\%$) throughout the system's lifetime (Fig. 6d–f). Relative humidity is lower behind the system and extends in area as the system progresses from initial to decaying stages (Fig. 6d–f).

4.3.2 Vertical structure

To examine the updraft, downdraft, and rear-to-front flow and hence outflow of the system, vertical cross sections are made along the lines AA', BB', and CC' of Fig. 4d–f. Figure 7a–c shows vertical cross sections of precipitation ($q_r + q_s + q_g$), equivalent potential temperature (θ_e), and wind along lines AA' (Fig. 4d), BB' (Fig. 4e), and CC' (Fig. 4f). Low θ_e (<340 K) is found from 2 to 8 km in front of the system (Fig. 7a). Below 1 km, high θ_e (>340 K) comes from the southeastern part and is uplifted over the northwestern low θ_e (<332 K). Behind the core of the mixing ratio, low θ_e (<340 K) extends below 5 km to the

Fig. 4 The *right panel* shows the simulated arc-shaped precipitation system of 26 April 2002 at **a** 1800 LST (developing), **b** 2100 LST (mature stage), and **c** 2300 LST (decaying stage). The *gray shading* indicates the mixing ratio of precipitation ($q_r + q_s + q_g$), and *vectors* represent the wind field at 1 km. The *left panel* shows the radar PPI observation on 26 April 2002 at **d** 1531 LST (initial stage), **e** 1936 LST (mature stage), and **f** 2147 LST (decaying stage). *Gray shading* indicates the rainfall intensity. *Lines AA'*, *BB'*, and *CC'* will be used in Fig. 7 and lines *BB'* and *EE'* will be used in Fig. 9



surface. During the mature stage, two upward velocity maximums of 5 and 14 m/s appear at heights of approximately 9 and 5 km and horizontal distance of approximately 95 and 25 km, respectively. The maximum vertical velocity is approximately 16 m/s, and the system develops up to 14 km (Fig. 7a) along the strong convergence line near the ground during the developing stage. Strongest vertical velocities ($w > 10$ m/s) occupy only a small fraction of the volume of the system, as also mentioned by Yuter and Houze (1995). During the mature stage, a stratiform region extends to about 150 km, and a secondary core of the maximum mixing ratio is seen at approximately

80 km behind the strongest core at around 6 km height. The mesoscale downdraft is weak (< 1 m/s) below the secondary core of the mixing ratio around 4 km (Fig. 7b). Rear-to-front flow extends to approximately 5 km depth and elongates about 50 km from the core of the mixing ratio at the developing stage. During the mature stage, maximum rear-to-front flow is 7 m/s (storm relative) at around 4 km. Outflow (≤ 18 m/s) produced by the weak rear-to-front flow converges with moist inflow just under the strong updraft core with a strong precipitation core. The intensity and area of the strongest core decrease in the decaying stage (Fig. 7c).

Fig. 5 **a** Radar-observed time series of the leading edge of the arc-shaped precipitation system. **b** CReSS-simulated time series of the leading edge of the arc-shaped precipitation system of 1 hour interval. The lines are drawn at the leading edge of the system

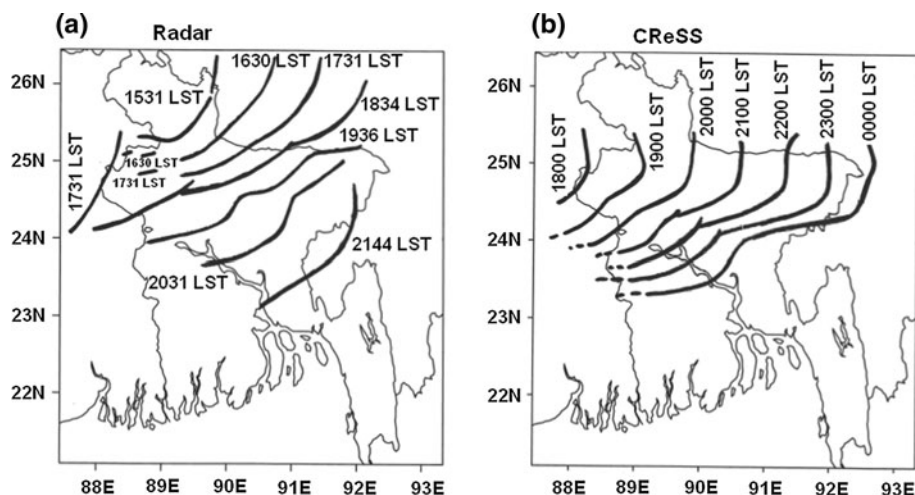


Table 1 Radar-observed and simulated characteristics of the arc-shaped precipitation system of 26 April 2002

Characteristics	Radar			CReSS		
	Initial	Mature	Decaying	Initial	Mature	Decaying
Propagation speed (m/s)	5	8	7	8	9	7
Length (km)	160	530	300	150	400	550
Propagation direction (degree)	SE (169)	SE (144)	SE (140)	SE (134)	SE (145)	SE (150)

Figure 7d–f shows the vertical profiles of average potential temperature, equivalent potential temperature, and saturated equivalent potential temperature of the 10-km \times 10-km grid box about 25 km ahead of the system along each line of the cross section during the developing, mature, and decaying stages. As clearly illustrated in the figure, the low levels are very moist, and the environment is unstable up to ~ 5 km. The average equivalent potential temperature after passage of the system is less than that in the same position up to ~ 4 km ahead of the system (not shown).

Figure 8a–c shows the average vertical profile of zonal wind (u) and updraft (w) during the initial, mature, and decaying stages. Areal averages are calculated for a 10-km \times 10-km area approximately 25 km ahead of the system and for a 6-km \times 6-km grid within the convective region of the system. Low-level (<1 km) easterlies ahead of the system decrease as the system progresses from initial to decaying stages. During the mature stage, the maximum low-level downdraft is ~ 2 m/s within the convective region at 2 km height. The downdraft has small depth at the decaying stage compared to the initial and mature stages. Updraft decreases within the convective region as the system progresses from the initial to decaying stages. Ahead of the system, a very weak updraft is observed about 2 km height. The environmental moderate shear is $3 \times 10^{-3} \text{ s}^{-1}$ between the 0 and 5 km levels and CAPE is

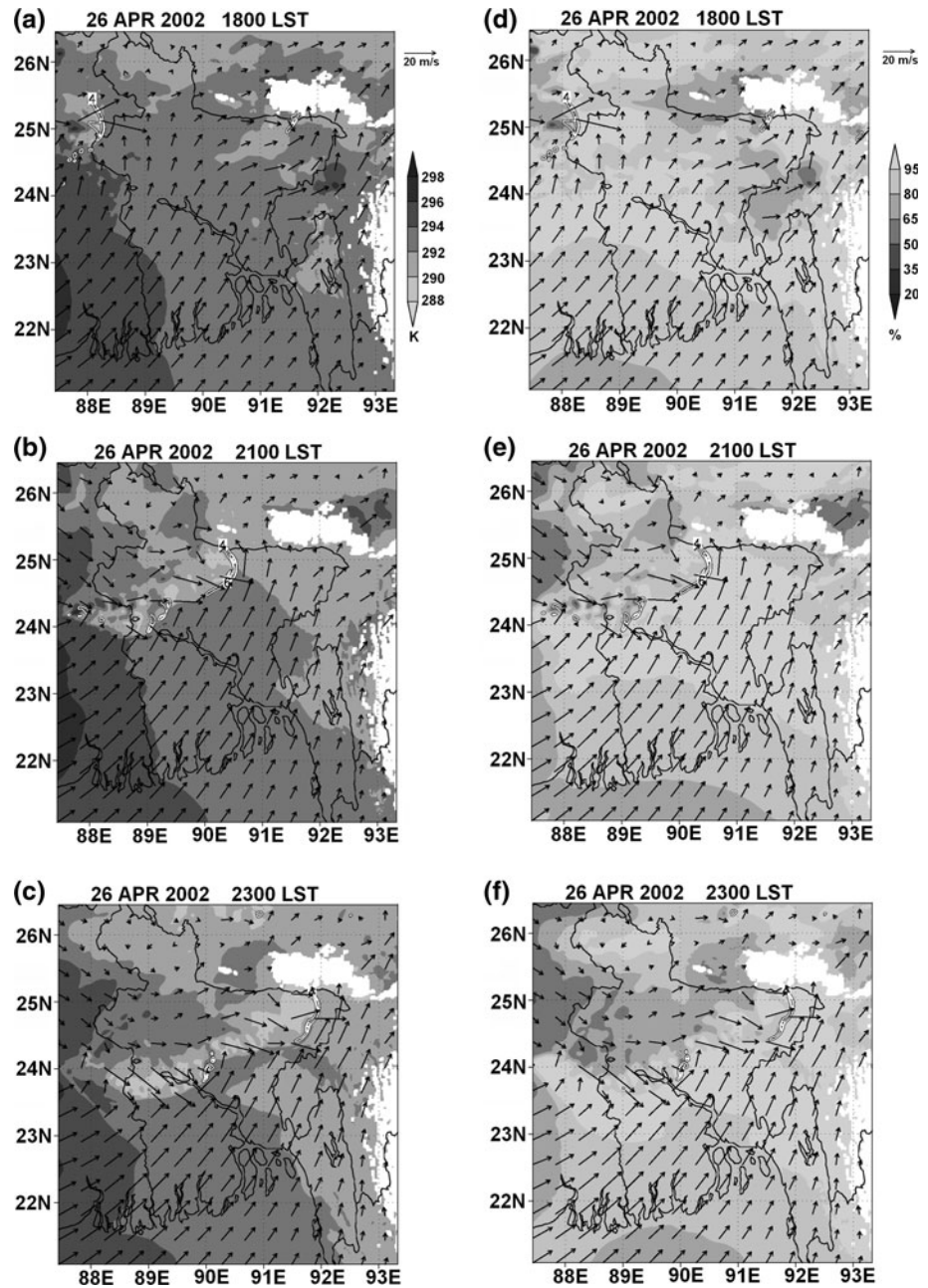
$2 \times 10^{-3} \text{ J/kg}$. The higher value of CAPE is found in the southwestern side of the system.

Figure 9 shows the vertical cross sections of the system along the lines BB' and EE' of Fig. 4e. The zonal component of inflow is 3 m/s and outflow is 24 m/s observed at 1 km level in the northeastern end of the system (Fig. 9a). The zonal component of inflow is 8 m/s and outflow is 15 m/s observed at 1 km level in the southwestern end of the system (Fig. 9b). The height of layer of inflow along BB' (northeastern end) is ~ 1.0 km and along EE' (southwestern end) is ~ 2.0 km. The extension of system along the cross section is 75 km in the southwestern end, whereas 140 km in the northeastern end.

5 Discussion

During the pre-monsoon period when arc-shaped precipitation systems develop, the low-level winds are southwesterly or southerly, leading to a well-marked shallow inflow of moisture from the Bay of Bengal to Bangladesh. In the mid-upper troposphere, moderate to strong westerly flow, often associated with the westerly jet, continues over the northeastern part of the Indian subcontinent (Weston 1972; Lohar and Pal 1995). These environmental conditions (low-level moisture and atmospheric instability) are

Fig. 6 CReSS-simulated temperature (*shading*), wind (*vector*), and mixing ratio of precipitation [contour (looks *thick line*), above 4 g/kg] on 26 April 2002 at **a** 1800 LST (developing stage), **b** 2100 LST (mature stage), and **c** 2300 LST (decaying stage). The simulated parameters are shown at 1 km height. **d–f** Same as (**a–c**) but for relative humidity (%) instead of temperature



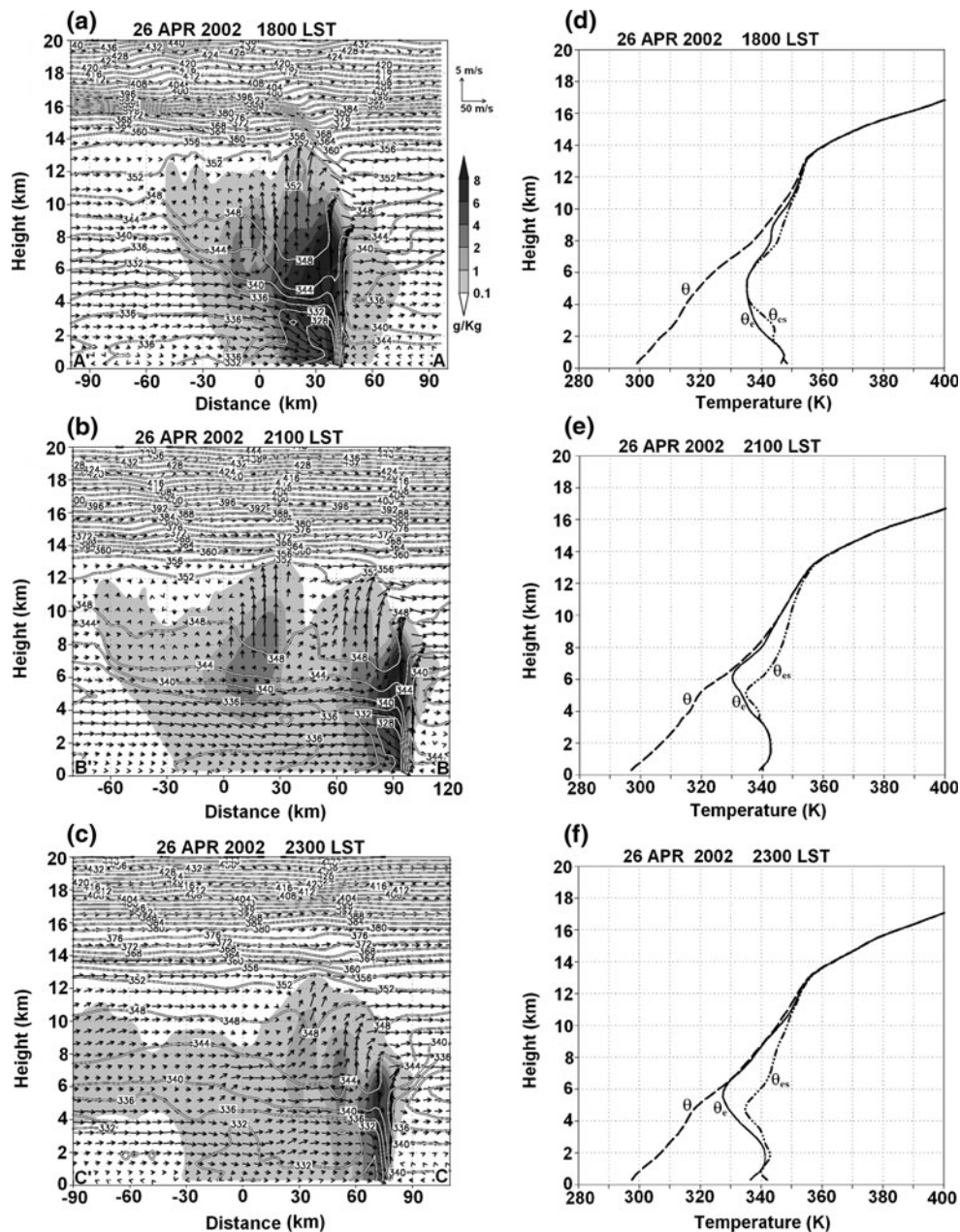
favorable for the development of convection during the pre-monsoon period.

As shown in Fig. 3, the development of young intense cells is found at the southwestern end of the system. These cells move northeastward and merge with the system. The extended stratiform region is found at the northeastern side of the system. In the southwestern side of the system, the low-level southwesterly or southerly wind carries moisture from the Bay of Bengal. The system propagates southeastward, with its northeastern end moving faster than the southwestern end, creating clockwise rotation. Two reasons are considered for the clockwise rotation of the system.

One is cold pool formation in the stratiform region. As mentioned in Sect. 4.3, behind the system, the temperature drop (~ 4 K) and its areal coverage in the northeastern end are larger than are those of the southwestern end. The outflow from the cold air mass to the front at the northeastern end of the system pushes that part of the line with greater strength than at the southwestern end. The other possible reason involves inflow to the system, which is against the outflow and stronger in the southwestern end than in the northeastern end (Fig. 9).

The propagation of the system can be explained by the rear-to-front flow. In the present case, as mentioned in Sect.

Fig. 7 Vertical cross sections along lines AA', BB', and CC' of Fig. 4d–f of the mixing ratio of precipitation ($q_r + q_s + q_g$, shading), wind (vector), and equivalent potential temperature (contour) at **a** 1800 LST (developing stage), **b** 2100 LST (mature stage), and **c** 2300 LST (decaying stage). Vertical profile of the average value of potential temperature (dash line), equivalent potential temperature (solid line), and saturated equivalent potential temperature (dash-dot line) at **d** 1800 LST (developing stage), **e** 2100 LST (mature stage), and **f** 2300 LST (decaying stage). The areal average is calculated for a 10-km \times 10-km grid box about 25 km ahead the leading edge of the system along lines AA', BB', and CC' of Fig. 4(d–f)



4.3, the weak (≤ 7 m/s, storm relative) rear-to-front flow starts from 5 km height, where relative humidity is high (about 60 %). In the moist environment, the small evaporation cooling explains the weak rear-to-front flow. To see the weak evaporation cooling, the temperature (T) and dew point temperature (T_d) are analyzed from the model results. The difference between pre-environmental T and T_d is approximately 5 °C around 1 km, which is smaller than values found in mid-latitude squall lines (Bluestein and Jain 1985; Ogura and Liou 1980; Fankhauser et al. 1992). Behind the system, an onion- or diamond-like shape is formed by the T and T_d curves (Ogura and Liou 1980; Johnson and Hamilton 1988). Ogura and Liou (1980)

demonstrated that T and T_d are separated by nearly 14 °C, and the relative humidity is 38 % around the 2-km level. In the present case, the separation of T and T_d is 5 °C at the same height, and the relative humidity is high (~ 60 %). These findings indicate that dry air intrusion and evaporation cooling are not significant. Shimuzu et al. (2008) noted that small evaporation cooling in a humid environment produced weak downdraft and hence weak rear-to-front flow. In turn, weak rear-to-front flow results in weak outflow, and the system propagates slowly.

Figure 10 presents a schematic illustration of a typical arc-shaped precipitation system that developed in Bangladesh during the pre-monsoon period. Pre-monsoon arc-

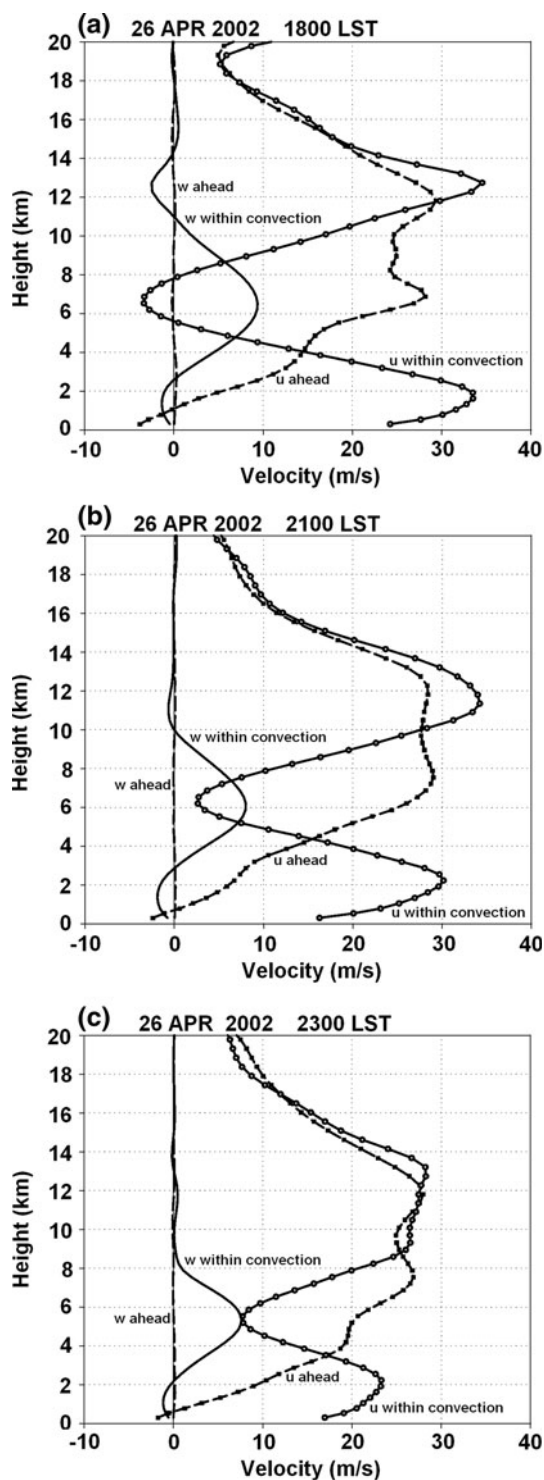


Fig. 8 Vertical profile of the average zonal wind (u) and updraft (w) at **a** 1800 LST (developing stage), **b** 2100 LST (mature stage), and **c** 2300 LST (decaying stage). The *dashed lines* represent zonal wind (u ; with circles) and updraft (w ; without marks) about 25 km ahead of the system. The *solid line* shows the same features as the *dashed line* but within convection. Averages are calculated for a 10-km \times 10-km grid box about 25 km ahead of the system and a 6-km \times 6-km grid box within the system along lines AA', BB', and CC' of Fig. 4d–f

shaped precipitation systems usually develop in the presence of moderate vertical wind shear over northern and northwestern parts of Bangladesh. Low-level warm moist air from the Bay of Bengal flows into the system. New cells develop in the southwestern end of the system, move northeastward, and merge with system and produce intense rainfall and become stratiform. The relatively strong outflow from the extended stratiform region at the northeastern end of the system creates clockwise rotation. This clockwise rotation is also enhanced by the relatively weak inflow component toward the leading edge of the system at the northeastern end.

6 Summary

The pre-monsoon arc-shaped precipitation system observed by radar on 26 April 2002 in Bangladesh (88.05–92.74°E, 20.67–26.63°N) was simulated using the Cloud Resolving Storm Simulator (CReSS) with a horizontal grid increment of 2 km. The Pennsylvania State University/National Center for Atmospheric Research Mesoscale Model (PSU/NCAR MM5) was used for downscaling. Japanese 25-year Reanalysis (JRA-25) data and National Oceanic and Atmospheric Administration (NOAA) Reynolds weekly mean SST data were used as initial and boundary conditions for MM5. Hourly outputs of the finest domain (5 km) of MM5 and NOAA Reynolds weekly mean SST data were used as the initial and boundary conditions for CReSS. This study is the first to simulate an arc-shaped precipitation system that was also observed by radar over Bangladesh.

New and intense cells of the arc-shaped precipitation system developed in the southwestern end of the convective line and propagated northeastward. Cells propagated northeastward and merged with system, and produced intense rainfalls and thus became stratiform. The simulation results indicate that low-level southwesterly or southerly warm moist air from the Bay of Bengal contributes to the development of new cells in the southwestern end of the system. The system propagates southeastward, and its northeastern end moves faster than the southwestern end, making the rotation clockwise. The slow propagation and clockwise rotation of the system coincide well with the radar observations. Cold pool formation in the stratiform region is considered one reason for the clockwise rotation. Behind the system, the temperature drop (~ 4 K) and its areal coverage are larger in the northeastern end than in the southwestern end. Outflow from the cold air mass to the front at the northeastern end of the system pushes that end with greater strength than the southwestern end. Another reason for the clockwise rotation is moist inflow to the system, which is against the

Fig. 9 Vertical cross sections of the average mixing ratio of precipitation ($q_r + q_s + q_g$, shading), wind (vector), and equivalent potential temperature (contour) along the lines **a** BB' (northeastern end of the system) and **b** EE' (southwestern end of the system) of Fig. 4e. The average is made across the lines BB' and EE' for the length of 30 km

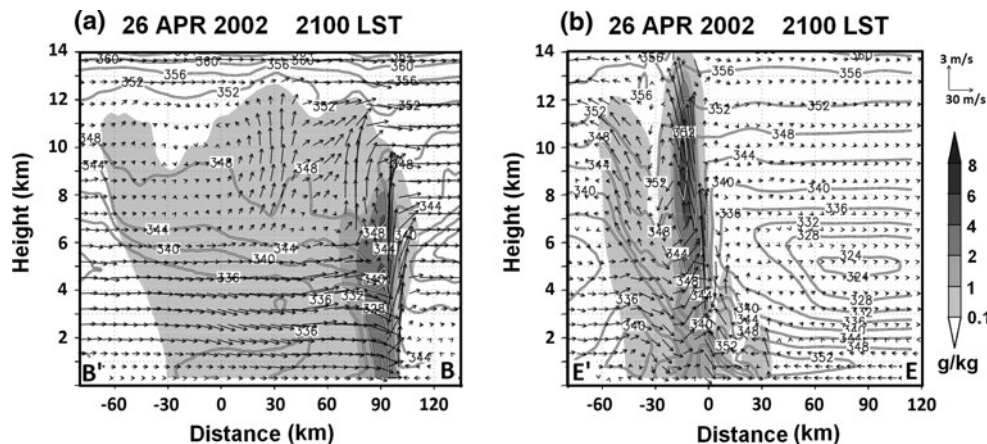
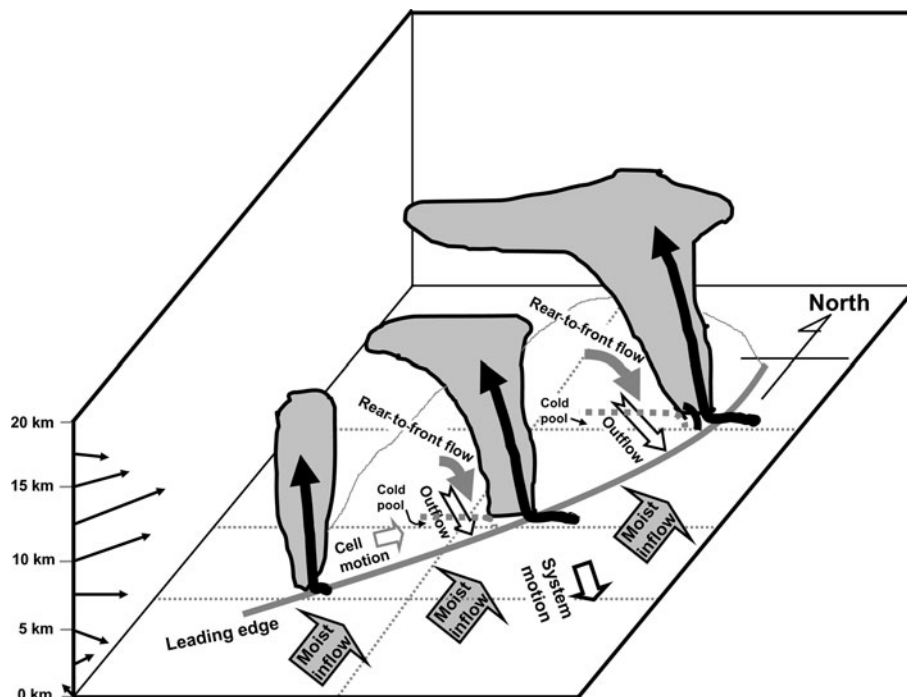


Fig. 10 Schematic illustration of the pre-monsoon arc-shaped precipitation system



outflow and stronger in the southwestern end than in the northeastern end. The propagation of the system can be explained by the weak (≤ 7 m/s, storm relative) rear-to-front flow in the moist environment.

The development processes of an arc-shaped precipitation system during the pre-monsoon period in Bangladesh can be explained as a balance of strong southwesterly or southerly moist inflow in the low altitudes and weak outflow in the rear of the system.

Acknowledgments The authors would like to thank the Bangladesh Meteorological Department for providing the radar data. The first author is fully supported by the Ministry of Education, Culture, Sports, Science, and Technology, Japan, as a doctoral student in the Graduate School of Environmental Studies, Nagoya University, Japan. The authors express their sincere gratitude to Dr. K. Tsubuki and Dr. T. Shinoda of the Hydrospheric Atmospheric Research Center

(HyARC), Nagoya University, for their invaluable suggestions. The authors would also like to thank Dr. Md. Nazrul Islam, Department of Physics, Bangladesh University of Engineering and Technology, Dhaka, Bangladesh, for his inspiration and invaluable suggestions. Thanks are also extended to T. Sano, T. Ohigashi, and S. Endo of HyARC, Nagoya University, for their invaluable help in data processing. The authors additionally thank all those involved with producing and disseminating the datasets and models used in this study. This study was partly supported by the Japan Science and Technology Corporation and a Grant-in-Aid for Scientific Research from the Japan Society for the Promotion of Science. This study is also partly supported by TRMM-RA6 of the Japan Aerospace Exploration Agency (JAXA).

References

Bluestein HB, Jain MH (1985) Formation of mesoscale lines of precipitation: severe squall lines in Oklahoma during the spring. *J Atmos Sci* 42:1711–1732

- Chowdhury MAM, De UK (1995) Pre-monsoon thunderstorm activity over Bangladesh from 1983 to 1992. *TAO* 6(4):591–606
- Dudhia J (1989) Numerical study of convection observed during winter monsoon experiment using a mesoscale two-dimensional model. *J Atmos Sci* 46:3077–3107
- Dudhia J (1993) A non-hydrostatic version of the Penn State—NCAR mesoscale model: validation tests and simulation of an Atlantic cyclone and cold front. *Mon Weather Rev* 121:1493–1513
- Fankhauser JC, Barnes GM, LeMore MA (1992) Structure of a midlatitude squall line formed in strong unidirectional shear. *Mon Weather Rev* 120:237–260
- Grell G (1993) Prognostic evaluation of assumptions used by cumulus parameterizations. *Mon Weather Rev* 121:764–787
- Hong SY, Pan HL (1996) Nonlocal boundary layer vertical diffusion in a medium range forecast model. *Mon Weather Rev* 124:2322–2339
- Islam MN, Uyeda H (2008) Vertical variations of rain intensity in different rainy periods in and around Bangladesh derived from TRMM observations. *Int J Climatol* 27:273–279. doi:[10.1002/joc.1585](https://doi.org/10.1002/joc.1585)
- Johnson RH, Hamilton PJ (1988) The relationship of surface pressure features to the precipitation and airflow structure of an intense midlatitude squall line. *Mon Weather Rev* 116:1444–1472
- Kataoka A, Satomura T (2005) Numerical simulation on the diurnal variation of precipitation over northeastern Bangladesh: a case study of a active period 14–21 June 1995. *SOLA* 1:205–208. doi:[10.2151/sola.2005-053](https://doi.org/10.2151/sola.2005-053)
- Litta AJ, Mohanty UC (2008) Simulation of a severe thunderstorm event during the field experiment of STORM programme 2006, using WRF-NMM model. *Curr Sci* 95(2):204–215
- Lohar D, Pal B (1995) The effect of irrigation on pre-monsoon season precipitation over the west Bengal, India. *J Clim* 8:2567–2570
- Ogura Y, Liou MT (1980) The structure of a midlatitude squall line: a case study. *J Atmos Sci* 37:553–567
- Peterson RE, Mehta KC (1981) Climatology of tornadoes of India and Bangladesh. *Arch Met Geoph Biokl Ser B* 29:345–356
- Rafiuddin M, Uyeda H, Islam MN (2010) Characteristics of monsoon precipitation systems in and around Bangladesh. *Int J Climatol* 30:1042–1055. doi:[10.1002/joc.1949](https://doi.org/10.1002/joc.1949)
- Shimuzu S, Uyeda H, Moteki Q, Takeshi T, Takaya M, Akaeda K, Kato T, Yoshizaki M (2008) Structure and formation mechanism on 24 May 2000 supercell-like storm developing in a moist environment over the Kanto Plain, Japan. *Mon Weather Rev* 136:2389–2407
- Tsuboki K, Sakakibara A (2002) Large-scale parallel computing of cloud resolving storm simulator. In: Zima HP et al (eds) *High performance computing*. Springer, Berlin, pp 243–259
- Weston KJ (1972) The dry-line of northern India and its role in cumulonimbus convection. *Q J Roy Meteorol Soc* 98:519–531
- Yamane Y, Hayashi T (2006) Evaluation of environmental conditions for the formation of severe local storms across the Indian subcontinent. *Geophys Res Lett* 33:L17806. doi:[10.1029/2006GL026823](https://doi.org/10.1029/2006GL026823)
- Yuter SE, Houze RA Jr (1995) Three-dimensional kinematic and microphysical evolution of Florida cumulonimbus. Part II: frequency distribution of vertical velocity, reflectivity and differential reflectivity. *Mon Weather Rev* 123:1941–1963